Defence Research and Development Canada
Recherche et développement pour la défense Canada

Profiles for Nodding Lasers – Implementations and Results

Sensing the World in an Intelligent Manner

G. Broten

Defence R&D Canada

Technical Memorandum

DRDC Suffield TM 2007-295

December 2007

Canada

Profiles for Nodding Lasers- Implementations and Results

Sensing the World in an Intelligent Manner

G. Broten
Defence R&D Canada – Suffield

Defence R&D Canada – Suffield

Technical Memorandum

DRDC Suffield TM 2007-295

December 2007

Principal Author

Original signed by G. Broten

G. Broten

Approved by

Original signed by S. Monckton

S. Monckton
Head/Autonomous Intelligent Systems Section

Approved for release by

Original signed by Dr. Paul D'Agostino

Dr. Paul D'Agostino
Chairman/Document Review Panel

Abstract

Historically, Defence R&D Canada investigated tele-operated vehicles, but in 2002 its research focus moved to general autonomy for land, air, and sea craft. Autonomy demands that the unmanned vehicle sense and represent its world as a prerequisite to intelligent navigation. A key element of Defence R&D Canada – Suffield's sensing suite is the nodding laser rangfinder that DRDC developed in conjunction with Scientific Instrumentation Ltd. The laser range data, returned from the nodding SICK laser, is the primary data source for DRDC's $2\frac{1}{2}$ D grid-map-based world representation. In its original form, the SICK laser nodded at a constant angular rate nodding profile. This implementation proved adequate for the fall 2005 Autonomous Land Systems demonstration, but the original implementation was utilitarian in nature. Although the constant angular rate nodding profile has yielded admirable results, analysis has shown that an adaptive nodding rate should theoretically yield even better results. Researchers at DRDC modified the nodding device's software to support user-definable, adaptive nodding profiles. Field tests exercised the new embedded software and revealed that the adaptive nodding system performed correctly. Experiments were then conducted to compare the performance of the constant angular rate profile to the performance of the adaptive nodding profile. These experiments revealed the performance of the adaptive nodding profile to be superior to that of the constant angular rate profile and the results were consistent with those predicted by theory and simulation.

Résumé

R&D pour la défense Canada examine les véhicules télé-opérés depuis des années mais en 2002, sa recherche a changé dorientation vers lautonomie générale pour les embarcations terrestres, aériennes et marines. Lautonomie demande, comme préalable à la navigation intelligente, que le véhicule sans pilote capte et représente son environnement géographique. Un élément clé de la technologie de détection de R&D pour la défense Canada est le télémètre laser basculant que RDDC a mis au point en collaboration avec Scientific Instrumentation Ltd. Les données télémétriques laser à distance, provenant du laser SICK basculant, est la source primaire de la représentation du monde basée sur la carte à quadrillage en $2\frac{1}{2}$ D de RDDC. Dans sa forme originale, le laser SICK basculait à un profil de vitesse angulaire de basculage constant. Cette implémentation sest démontrée adéquate durant la démonstration des Systèmes terrestres autonomes à lautomne 2005 mais limplémentation originale était de nature utilitaire. Bien que le profil de vitesse angulaire de basculage constant ait produit des résultats admirables, les analyses ont montré que la vitesse de basculage adaptive devrait théoriquement produire de meilleurs résultats. Les chercheurs de RDDC ont modifié le logiciel de lappareil de balayage pour soutenir des profils de balayage adaptifs définis par lutilisateur. Les essais pratiques ont utilisé le nouveau logiciel intégré et ont révélé que le système de balayage adaptif fonctionnait correctement. On a ensuite effectué des expériences pour comparer le rendement du profil de vitesse angulaire constant avec celui du profil de balayage adaptif. Ces expériences ont révélé que le rendement du profil de balayage adaptif est supérieur à celui du profil de vitesse de balayage angulaire constant et les résultats concordaient avec ceux prédits par la théorie et la simulation.

This page intentionally left blank.

Executive summary

Profiles for Nodding Lasers- Implementations and Results

G. Broten; DRDC Suffield TM 2007-295; Defence R&D Canada – Suffield; December 2007.

Background: Defence R&D Canada researches Autonomous Intelligent Systems as defined by the DRDC Technology Investment Strategy (TIS) where the TIS defines autonomy as *"...automated or robotic systems that operate and interact in the complex and unstructured environments of the future battlespace"*. Sensing is key to autonomous operations since it allows an unmanned vehicle (UxV) to construct a world representation and then use this representation to perform intelligent navigation. Previous unmanned ground vehicle (UGV) trials relied upon nodding lasers using constant angular nodding profiles and although this configuration produced good results, theory and simulations indicate that adaptive nodding profiles should yield provide better map statistics at the map's extremities. Researchers at DRDC modified the nodding device's embedded software to support adaptive nodding profiles and compared this configuration with the original constant angular rate profile.

Principle Conclusions: Field tests were conducted and the performance of constant angular rate profile was compared to that of the adaptive nodding profile. These experiments revealed the adaptive nodding profile yielded $2\frac{1}{2}$ D terrain maps with lower grid element standard deviations and this improvement was most significant at the map extremities.

Significance of Results: Laser rangefinder based terrain maps are historically myopic due to the limited range of the laser. Myopic terrain maps are characterized by poorly defined elevation data at the map extremities and do not allow the UGV to *aim high in steering*, meaning it doesn't look far ahead. Thus, the UGV is forced to make last second decisions to avoid obstacles. The adaptive nodding profile results in a terrain map that is less myopic than the terrain map produced using the constant angular rate nodding profile. This results in a better representation of distant obstacles, thereby expanding the map's useful size. Just as human drivers benefit from aiming high in steering, overall UGV performance is improved with an expanded terrain map as obstacles are identified sooner and obstacle avoidance is more intelligent.

Future Results: The Raptor vehicle originally featured a single laser, while the current setup consists of two nodding lasers. The move from a single laser to dual lasers increased the density of range data, but the density is still relatively low. Future work will investigate laser ranging devices with higher data densities and compare their performance to that of the current dual laser configuration.

Sommaire

Profiles for Nodding Lasers- Implementations and Results

G. Broten ; DRDC Suffield TM 2007-295 ; R & D pour la défense Canada – Suffield ; décembre 2007.

Contexte : R & D pour la défense Canada effectue la recherche sur les Systèmes intelligents autonomes tels que définis par la Stratégie dinvestissement technologique (SIT), laquelle définit autonomie comme *" systèmes automatisés ou robotiques qui opèrent et interagissent dans les environnements complexes et non structurés des futurs champs de bataille"*.. La détection est la clé des opérations autonomes puisquelle permet à un véhicule autonome (UxV) de construire une représentation du monde et dutiliser cette représentation pour naviguer intelligemment. Des essais antécédents sur les véhicules terrestres sans pilote reposaient sur des lasers basculants qui utilisaient des profils angulaires de basculage constants ; bien que cette configuration ait produit de bons résultats, la théorie et les simulations indiquent que les profils de basculage adaptifs devraient produire de meilleures statistiques cartographiques aux extrémités de la carte. Les chercheurs de RDDC ont modifié lappareil de basculage intégré dans le logiciel pour soutenir des profils de basculage adaptifs et ont comparé cette configuration avec le profil de vitesse angulaire constant.

Conclusions principales : On a conduit des essais pratiques et on a comparé le rendement du profil de vitesse angulaire constant à ceux du profil de basculage adaptif. Ces expériences ont révélé que le profil de basculage adaptif produisait des cartes morphographiques en $2\frac{1}{2}$ D ayant des écarts types déléments de grille moindres et cette amélioration était plus importante aux extrémités de la carte.

Portée des résultats : Les cartes morphographiques basées sur les télémètres lasers sont traditionnellement myopes à cause de létendue limitée du laser. Les cartes morphographiques myopes sont caractérisées par des données daltitude mal définies et les extrémités des cartes ne procurent pas au véhicule terrestre sans pilote un champ de vision en hauteur à la conduite, ce qui veut dire que le champ de vision est limité. Le véhicule est, de cette manière, forcé de prendre des décisions de dernière minute pour éviter les obstacles. Le profil de basculage adaptif produit une carte morphologique qui est moins myope que la carte morphologique produite par le profil de vitesse angulaire de basculage constant. Ceci résulte en une meilleure représentation dobstacles distants et étend par conséquent la zone utile de la carte. De la même manière que les chauffeurs humains ont tout avantage à avoir un champ de vision en hauteur au volant, le rendement global du véhicule terrestre sans pilote est amélioré par la carte morphographique étendue qui identifie les obstacles plus tôt et évite les obstacles plus intelligemment.

Perspectives davenir : Le véhicule Raptor ne comportait à lorigine quun seul laser alors que lappareillage actuel consiste en deux lasers basculants. Le changement dun laser à deux lasers augmente la densité des données télémétriques mais la densité demeure relativement faible. Des travaux futurs examineront les appareils de télémétrie laser ayant des densités de données plus hautes et compareront leur rendement à celui de la configuration à deux lasers actuelle.

Table of contents

Abstract i

Résumé i

Executive summary iii

Sommaire iv

Table of contents v

List of figures vii

List of tables viii

1 Introduction 1

2 Implementation of the Uniform Sample Distance Profile 2

2.1 Geometry and Mathematics 2

2.2 Software for the Scientific Instrumentation Ltd. Nodding Device 3

2.2.1 Booting the Nodding Device 3

2.2.2 Compiling the Application 4

2.2.3 Modifications to the control software 5

2.3 Interface with Miro Framework 6

3 Experiments and Results 7

3.1 Setup 7

3.2 Experimental Theory 8

3.2.1 Physical Geometry of the Laser Configuration 9

3.2.2 Adaptive Nodding 9

3.2.3 Quantifying the Laser Configuration's Performance using Terrain Maps 10

3.3 Initial Experiments 12

3.3.1 Map Performance, Single Fixed Laser 12

3.3.2 Map Performance, Dual Fixed Lasers 15
3.3.3 Map Performance, Single Fixed Laser and a Nodding Laser 16
3.3.4 Discussion 18
3.4 Terrain Map Performance for a 24 m Look-ahead Distance 19
3.4.1 Map Performance, Single Fixed Laser 20
3.4.2 Map Performance, Dual Fixed Lasers 21
3.4.3 Map Performance, Single Fixed Laser and a Nodding Laser 21
3.4.4 Map Performance, Adaptive Nodding 23
3.4.5 Discussion 24
4 Conclusions 25
References 27

List of figures

Figure 1: Scientific Instrumentation Nodding Device 1

Figure 2: Geometry of a Nodding Laser Rangefinder 2

Figure 3: Booting the Nodding Device 4

Figure 4: Services Flow Diagram 6

Figure 5: Services Flow Diagram 8

Figure 6: The Maximum Look-ahead Distance's Relationship to the Laser Mount Angle 9

Figure 7: Constant Angular Rate of $\frac{30^\circ}{sec}$, $90^\circ \rightarrow 15^\circ$ (Left), $15^\circ \rightarrow 2^\circ$ (Right) . . . 10

Figure 8: Uniform Sample Density with $d = 0.20$ m, Theoretical (Left), Achievable (Right) 10

Figure 9: Typical Ego-Centric Terrain Map 11

Figure 10: Ego-Centric Terrain Map, Stationary Vehicle, Laser at -10° 12

Figure 11: Ego-Centric Terrain Map, Mid Traverse and Return to Start, Laser at -10° 13

Figure 12: Ego-Centric Terrain Map, Mid Traverse and Return to Start, Laser at -20° 13

Figure 13: Ego-Centric Terrain Map, Mid Traverse and Return to Start, Laser at -30° 14

Figure 14: Egocentric Map for Dual Lasers at -10° and -20° 15

Figure 15: Egocentric Map for a Nodding Laser, Stationary Vehicle 16

Figure 16: Typical Ego-Centric Terrain Map with a 24 m Look-ahead distance . . . 19

Figure 17: Terrain Map with Zones, 24 M Look-ahead Distance (left) and 12 m Look-ahead Distance (right) 20

Figure 18: Terrain Map with Zones, Nod Angle $-5^\circ \rightarrow -30^\circ$ 24

List of tables

Table 1: Uniform Sample Distance Lookup Table 6

Table 2: Single Laser, Forward Motion only 14

Table 3: Dual Lasers, Forward Motion only, Look-ahead distance 12 m 16

Table 4: Nodding Angles for Experiments with a Fixed Laser Look-ahead distance of 12 m 17

Table 5: Constant Angular Nodding Rates for the Experiments 17

Table 6: Nod Angle $-20°$ to $-40°$, Fixed Laser Look-ahead distance 12 m 17

Table 7: Nod Angle $-10°$ to $-40°$, Fixed Laser Look-ahead distance 12 m 18

Table 8: Nod Angle 0 to -40 Degrees, Fixed Laser Look-ahead distance 12 m . . . 18

Table 9: Single Laser, Forward Motion only 20

Table 10: Dual Lasers, Forward Motion only, Look-ahead distance 24 m 21

Table 11: Nodding Angles for Experiments with a Fixed Laser Look-ahead distance of 24m 21

Table 12: Nod Angle $-5°$ to $-30°$, Fixed Laser Look-ahead distance 24 m 22

Table 13: Nod Angle $-5°$ to $-25°$, Fixed Laser Look-ahead distance 24 m 22

Table 14: Nod Angle $-5°$ to $-20°$, Fixed Laser Look-ahead distance 24 m 22

Table 15: Nod Angle $-5°$ to $-15°$, Fixed Laser Look-ahead distance 24 m 23

Table 16: Dual Lasers, Adaptive Nodding, Look-ahead distance 24 m 23

1 Introduction

An unmanned autonomous vehicle (UxV), navigating unstructured and outdoor environments, must quickly create an adequate local representation of its world. Defence R&D Canada's current state-of-the-art world representation [1, 2], similar to the Stanford Stanley robot that won the DARPA Grand Challenge [3], requires 3 dimensional sensing. This configuration can be achieved via active sensors or through passive sensing. Active sensors, such as laser rangefinders, have long been preferred by the UxV community because of their accuracy, reliability and repeatability. The ubiquitous SICK laser rangefinder is commonly used on unmanned ground vehicles (UGV), but this device is 2 dimensional and can only scan along a line or slice of terrain. Under the Autonomous Land Systems (ALS) project DRDC contracted Scientific Instrumentation Ltd. to develop a nodding device for the 2-D SICK LMS 291 laser rangefinder. The nodding device rotates the SICK laser about the horizontal thereby creating a 3-D device that scans an area. Figure 1 shows the nodding device for the SICK laser.

Figure 1: *Scientific Instrumentation Nodding Device*

Area scanning allows for the generation of a navigable world representation without requiring vehicular motion. A nodding laser also creates multiple data sets, from varying perspectives, that result in a more accurate and reliable statistical world representation [4].

DRDC researchers investigated the operation of a nodding SICK laser rangefinder, its benefits and performance, and in a previous publication proposed two modes of operation known as nodding profiles, which the nodding device could implement [5]. The first nodding profile simply nods the SICK laser at a constant angular rate (CAR). This simplest of nodding profiles was implemented for and successfully used in the September, 2005 Autonomous Land Systems (ALS) demonstration. The second proposed nodding profile uses adaptive nodding to implement a uniform sample distance[1] (USD). The USD profile nods the laser in such a manner that terrain sampling occurs at a uniform depth, whereas the CAR profile creates a dense sample for angles nearing vertical, but at angles near the horizon few samples are acquired. Thus, in theory, the USD profile should improve the overall UGV's

[1] Also known as the uniform sample depth.

ability to model the distant world. This USD profile was investigated via simulations, but wasn't implemented for the ALS demonstration.

Additionally, for the fall 2005 Demonstration the Raptor UGV employed a single laser rangefinder. Subsequent modifications to the Raptor platform allowed for the mounting of two laser rangefinders. By increasing the number of lasers, the data densities are also increased which, from a theoretical point of view, should yield better terrain map statistics.

This publication covers DRDC's dual laser configuration, the nodding SICK laser implementation, and provides experimental results that quantify each configuration's performance. The report is divided into 4 sections. Section 2 details the uniform sample distance profile implementation. The experiments testing dual laser configuration, the USD profile, the analysis and the results are provided in Section 3. The report finishes with the conclusions given in Section 4.

2 Implementation of the Uniform Sample Distance Profile

2.1 Geometry and Mathematics

The geometry of a vehicle mounted laser rangefinder is shown in Figure 2. As shown in this figure, rotation of the SICK laser device moves the laser from its previous position denoted by θ_i, through an angular displacement of $\delta\theta$ to a new sampling position at θ_{i+1}. This new sample position is controlled by the SICK laser sweep period, τ, and the angular rotational rate, ω, of the nodding device since the angular displacement is given by:

$$\delta\theta = \tau \times \omega \tag{1}$$

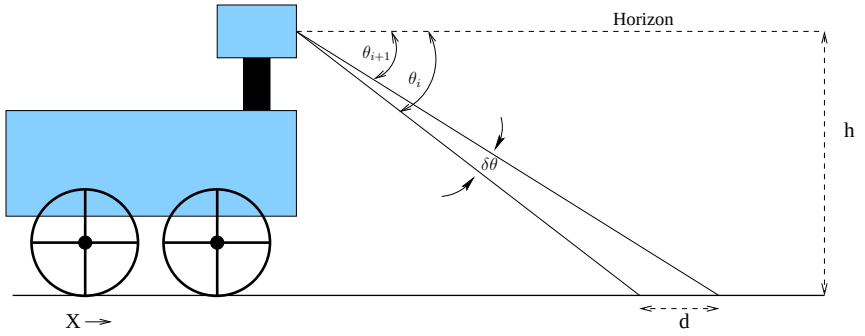

Figure 2: *Geometry of a Nodding Laser Rangefinder*

Using the geometry shown in Figure 2 it is simple to derive the relationship between θ_i, θ_{i+1} and the distance, d, between the two sampled terrain slices. Using triangulation:

$$d = \frac{h}{\tan(\theta_{i+1})} - \frac{h}{\tan(\theta_i)} \tag{2}$$

For the USD profile the distance, d, is specified as a constant and the starting angle, θ_i, is known. Thus, rearranging the above equation and solving for the new angle, θ_{i+1}, yields:

$$\theta_{i+1} = \arctan\left(\frac{h \times \tan(\theta_i)}{h - d \times \tan(\theta_i)}\right) \tag{3}$$

Thus, for any defined sample distance and an initial angle, the new angle that achieves the uniform sample distance can be calculated. The angle through which the nodding device must sweep is given by $\delta\theta = \theta_{i+1} - \theta_i$. Noting that the SICK laser has fixed sweep period of τ, the nodding mechanism's required angular rate is given by:

$$\omega_{sweep} = \frac{\delta\theta}{\tau} \tag{4}$$

2.2 Software for the Scientific Instrumentation Ltd. Nodding Device

Scientific Instrumentation Ltd. created a nodding device for the SICK LMS 291 laser, which is shown in Figure 1. This nodding device consists of:

- An embedded Motorola 68360 micro-controller.
- A stepper motor, connected to a shaft, that rotates the SICK laser.
- An optical encoder, also connected to the shaft, that provides feedback with respect to the shaft's rotational position.
- Ethernet hardware for interfacing with the 68360 micro-controller.

The embedded 68360 processor runs the open source RTEMS real-time operating system [6]. Using the GNU tools, source code is compiled and linked into an executable file, which is then downloaded to the 68360 micro-controller. The contract between DRDC and Scientific Instrumentation Ltd. specified that the source code for the nodding device be supplied as a contract deliverable, thus researchers have the flexibility to update, and modify the embedded software.

2.2.1 Booting the Nodding Device

Loading the control software into the nodding device's micro-controller and booting the system is a simple process. The boot process has five major stages, as is shown in Figure 3.

1. The micro-controller broadcasts a DHCP request across the network.
2. If the MAC address, encoded in the DHCP request, matches the software server's dhcpd.conf list, it replies with an IP address.
3. Once the micro-controller has acquired a valid IP address it uses TFTP [2] to request the application.
4. The application, defined in the dhcpd.conf list, is transferred to the micro-controller.
5. The micro-controller boots into the application.

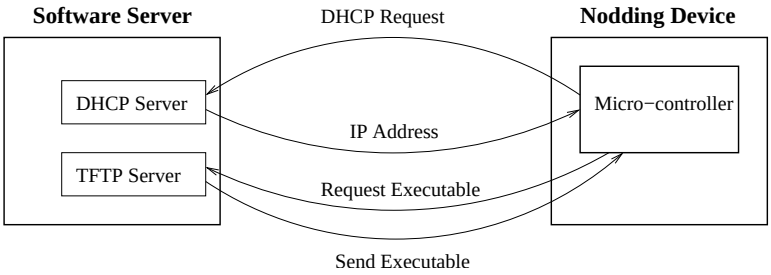

Figure 3: *Booting the Nodding Device*

Using this dynamic process, where the nodding device's application code resides on the software server, it is simple to modify the nodding device's capabilities.

2.2.2 Compiling the Application

Before the application can be compiled the GNU/Linux x86 development host tools, for the M68k series of micro-controllers, must be installed. The required development host applications include: GCC, G++, Make, Autotools, libraries and the GDB debugger, and they are available from the RTEMS website [7]. Instructions for their installation are located on DRDC Suffield's AISS Wikipage [8].

Once the development host has been configured the source code for the RTEMS operating system must be installed, configured and compiled. Keys aspects of this process include:

- Boot strapping the configuration process.
- Configuring RTEMS to support m68k-rtems libraries and the gen68360 processor.
- Making and installing.

Complete details on the configuration process are also located on the DRDC-Suffield AISS Wikipage [8].

[2] Trivial File Transfer Protocol.

Scientific Instrumentation Ltd's original control software included both the source code files and the Makefile required by the compiling and linking process. Before compiling can occur the location of the host development tools and the RTEMS source must be defined. These locations are defined as follows:

1. export PATH=/opt/rtems-4.6/bin/ - Defines the host development tools root directory.
2. RTEMS_MAKEFILE_PATH=/opt/rtems/m68k-rtems/gen68360 - This directive is located in the application's Makefile and defines the root directory of the RTEMS source.

2.2.3 Modifications to the control software

The nodding device's default control software supported only a CAR, so researchers at DRDC modified the control software to also support the USD profile.

The stepper motor is driven by a pulse width modulation scheme where the angular rotation rate is proportional to the pulse rate. Thus, for a constant angular rate, specified in deg/sec, the control software simply sets the pulse rate to the appropriate value. Noting that there are $\frac{360^\circ}{rev.}$ and $\frac{5000\ steps}{rev.}$, the conversion to a pulse rate is given by:

$$P\ \frac{pulses}{sec} = Rate \times \frac{5000}{360} \tag{5}$$

The USD profile requires a more sophisticated implementation. As shown in Section 2.1, sampling the terrain at a uniform distance requires an adaptive nodding rate. To sample at a uniform distance the next rotational angle, θ_{i+1}, must be calculated using the current angle, θ_i and nodding device's mount height, h. Referring to the mathematics in Section 2.1, the difference angle, $\delta\theta$, can be calculated and the corresponding rotational rate, ω_{sweep}, can be found. Although these mathematics are straight forward, the limited processing power of the Motorola 68360[3] and the requirement for three trigonometric functions may preclude their real-time calculation. To avoid any potential processing power issues DRDC researchers optimized the USD profile's implementation. Researchers noted that both the vehicle geometry and the sample distance are nominally static, meaning they don't vary once a UGV configuration has been specified. Thus, it is possible to create a pre-calculated lookup table that reflects this configuration. When the nodding device is commanded into the USD mode it is also given its mounting height and the specified sample distance. Substituting these values into the equations from Section 2.1 the rotational rate, required to achieve the next sample angle, is determined for every possible encoder angle and this value is stored in the lookup table[4]. Table 1 shows the form of this lookup table.

[3]The micro-controller has a clock speed of 25 MHz and only supports integer math.

[4]At angles near the horizon, where the calculated $\delta\theta$ is less than the encoder resolution, the encoder resolution is substituted as $\delta\theta$.

Angle, θ Degrees	**Encoder** Counts	**Rotational Rate**, ω deg/sec
0.0	0	ω_0
0.072	1	ω_1
0.144	2	ω_2
0.216	3	ω_3
⋮	⋮	⋮
14.976	200	ω_{200}

Table 1: *Uniform Sample Distance Lookup Table*

Thus, using the pre-calculated lookup table, the require rotational rate required is determined by simply selecting the rate that corresponds to the current encoder count.

2.3 Interface with Miro Framework

DRDC has developed a complete suite of applications that allow a UGV to operate autonomously. All applications have been developed under an adapted and extended version of the Miro framework [9, 10] known as the "Architecture for Autonomy" (AFA) [11, 12, 13]. The flow diagram in Figure 4 shows the various services that cooperatively implement autonomous capabilities.

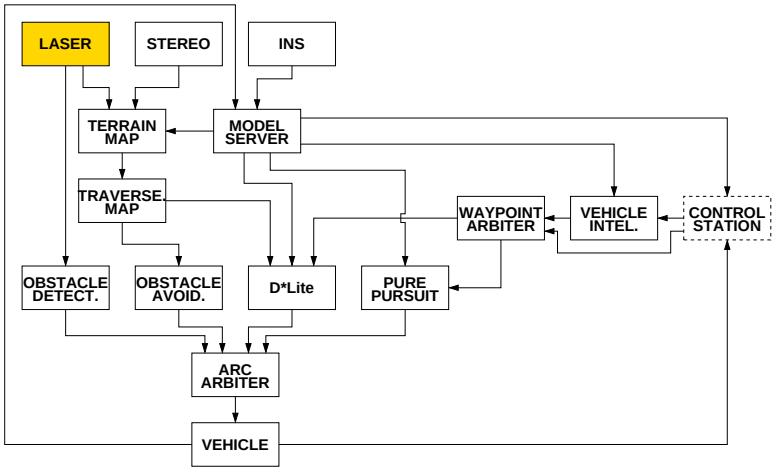

Figure 4: *Services Flow Diagram*

Highlighted in Figure 4 is the Laser application that embodies three key functions:

1. Implements the device drive that controls the nodding device and receives data from the SICK laser.
2. Converts the received range data from its native format into a generic 3-D range representation.

3. Publishes the range data as a CORBA Range3dLaserIDL event [11].

The existing Miro Laser driver was extended to support the USD profile. To command the nodding device into the USD profile the Laser driver must transfer the following information to the nodding device:

- The Laser's mount height above the ground plane, and
- The sample distance.

Upon sending the USD profile command the nodding device will create the USD lookup table[5] and send range data as usual.

3 Experiments and Results

Theory and simulations reveal a number of interesting laser rangefinder facts [4, 5]:

- The range data's uncertainty is proportional to the measured range,
- Higher data densities yield a terrain map with more relevant statistical properties, and
- The laser(s) configuration highly influences the terrain map's data densities.

Experiments were designed and performed that investigated the effects of a variety of laser rangefinder configurations. Each configuration yields a *look-ahead* distance; the maximum distance at which the terrain is sampled. Given that this research aims to maximize the look-ahead distance, the dual nodding configuration was not investigated as it does not help achieve this goal. Maximizing the look-ahead distance requires that the regions most distant from the vehicle be continuously sampled and this objective is best implemented by having at least one fixed laser sampling distant terrain. The configurations tested include:

- A single laser rangefinder at a fixed angle,
- Dual laser rangefinders at fixed angles, and
- A laser rangefinder at a fixed angle and a nodding laser.

These configurations were tested at two separate maximum look-ahead distances.

3.1 Setup

For these experiments DRDC used its Raptor UGV, as shown in Figure 5. The Raptor UGV hosts a complete application suite that allows the vehicle to autonomously operate in low complexity, outdoor environments.

For the experiments the following sensors where used:

[5] On the Motorola 68360 is process takes approximately 2 minutes to complete.

Figure 5: *Services Flow Diagram*

- Novatel Span INS, providing the vehicle's position and orientation.
- Two SICK lasers that return range data with respect to the terrain in front of the Raptor UGV.

A series of experiments were performed, with each experiment conducted as follows:

1. Start the Raptor UGV, drive directly forward approximately 50 m, and then backup to the starting point.
2. While the experiment is in progress, log laser and pose data to a file.
3. Offline, replay this data into the terrain map process via the Miro LogPlayer.
4. Analyze the resulting map density and standard deviation.

These experiments were conducted with dual lasers mounted on top of the Raptor UGV and both lasers acquired range data. Depending on the type of analysis performed the data from only a single laser, or from both lasers may be used.

3.2 Experimental Theory

The following sections provide details with respect to the parameters that affect the experiments and how the experimental results were quantified.

3.2.1 Physical Geometry of the Laser Configuration

The maximum look-ahead distance defines the terrain map's maximum useful size. The maximum look-ahead distance is a function of both the SICK laser's maximum range and of the mounting geometry. Figure 6 illustrates the geometric relationship between the laser's mount height, the mount angle angle and look-ahead distance. The bottom geometry shows that a -5° mount angle[6] yields a 24 m look-ahead distance, which is near the SICK LMS 291 laser's maximum range of 30 m. Also illustrated is the -10° mount angle that results in a look-ahead distance of 11.9 m.

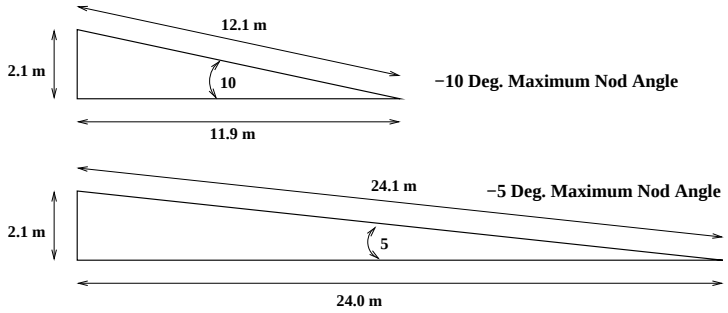

Figure 6: *The Maximum Look-ahead Distance's Relationship to the Laser Mount Angle*

3.2.2 Adaptive Nodding

In theory and simulation the USD profile offers advantages over the CAR profile. The CAR profile, with its non-uniform sampling profile, sparsely samples distant terrain, whereas the USD profile attempts to equally sample the terrain in front of the vehicle. Thus, the USD profile should improve the Raptor's ability to reliably detect distant obstacles. Figure 7 shows the theoretical distance between samples for the CAR profile, while Figure 8 shows the theoretical inter-sample distance for the USD profile[7]. These figures clearly illustrate the differences between the two nodding profiles. At high angles the CAR profile yields a sample distance near 0.02 m, but this sample distance increases exponentially as the nodding angle decreases. For nodding angles above $\simeq -50^\circ$ the intra-sample distance is greater than 0.02 m and at angles above approximately $\simeq -5^\circ$ it is greater than 1 m. By contrast, the USD profile maintains the 0.02 m sample distance through all nodding angles up to $\simeq -20^\circ$. At this point the encoder resolution of 0.072° has been reached and the nodding device can no longer accurately rotate to the required angles. Thus, the intra-sample distance increases but never exceeds a value of 0.6 m. These figures also reveal the two nodding profiles exhibit opposite sample density properties: the CAR profile's density is greatest at high nod angles, whereas the USD profile's density is highest at low angles.

The USD profile's density distribution should yield a more accurate world representation for distant terrain. To test this hypothesis terrain map representations were created and analyzed.

[6] This corresponds to 5° below the horizon.

[7] For both of these simulations the nodding laser has a mount height of 2.0 m.

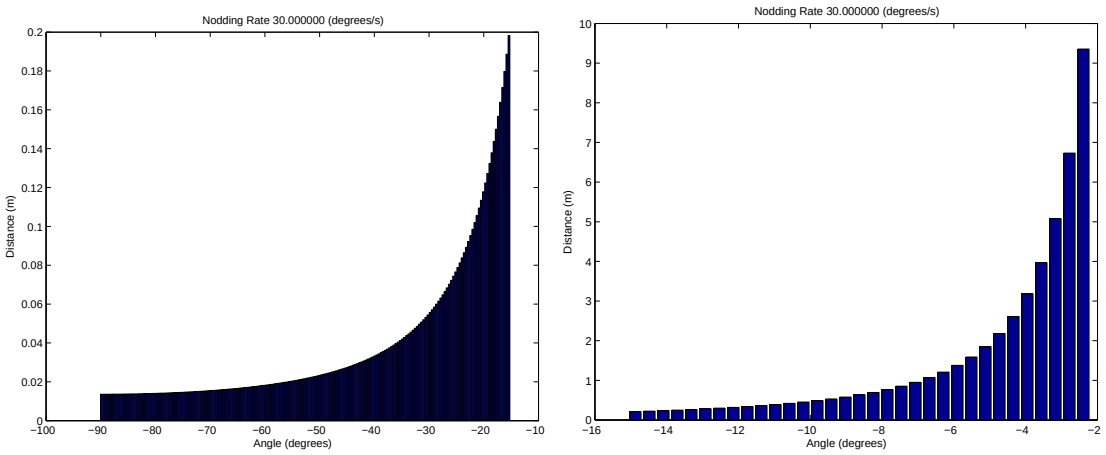

Figure 7: *Constant Angular Rate of* $\frac{30^\circ}{sec}$, $90^\circ \rightarrow 15^\circ$ *(Left),* $15^\circ \rightarrow 2^\circ$ *(Right)*

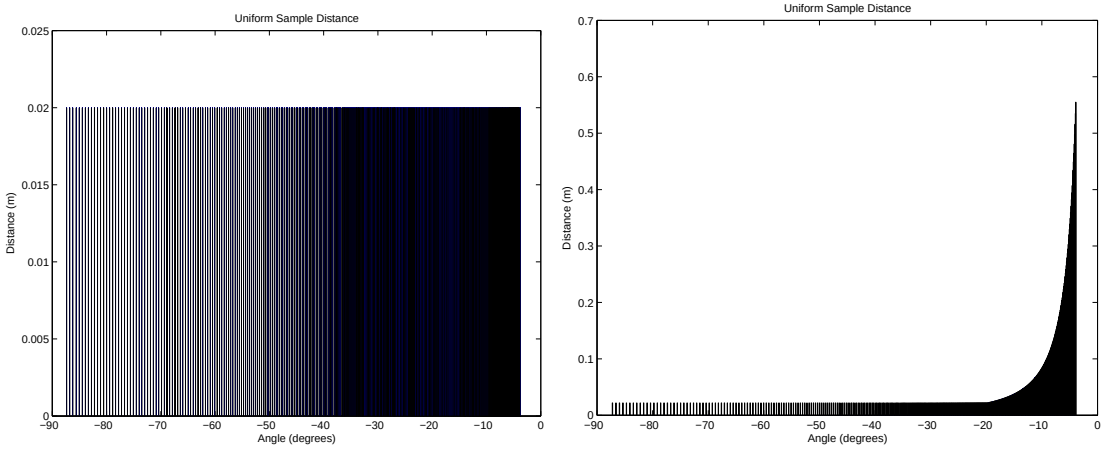

Figure 8: *Uniform Sample Density with* $d = 0.20$ *m, Theoretical (Left), Achievable (Right)*

3.2.3 Quantifying the Laser Configuration's Performance using Terrain Maps

A terrain map represents the world through a rectangular array of regions, where each grid element contains the mean elevation for the given terrain patch [2]. The mapping process statistically fuses the range data, acquired from the nodding SICK laser, into the appropriate terrain map grid elements [5]. Figure 9 shows a typical, ego-centric terrain map where color represents elevation: red is low, green is flat and blue is high. This terrain map represents the terrain 30 m on either side of the vehicle and to a distance of 30 m in front of the vehicle.

This figure contains additional map markups that illustrate the map zones known as *near*, *medium* and *far*. These zones are used in quantifying the map's performance. For each experiment the average map density and average grid element standard deviation was cal-

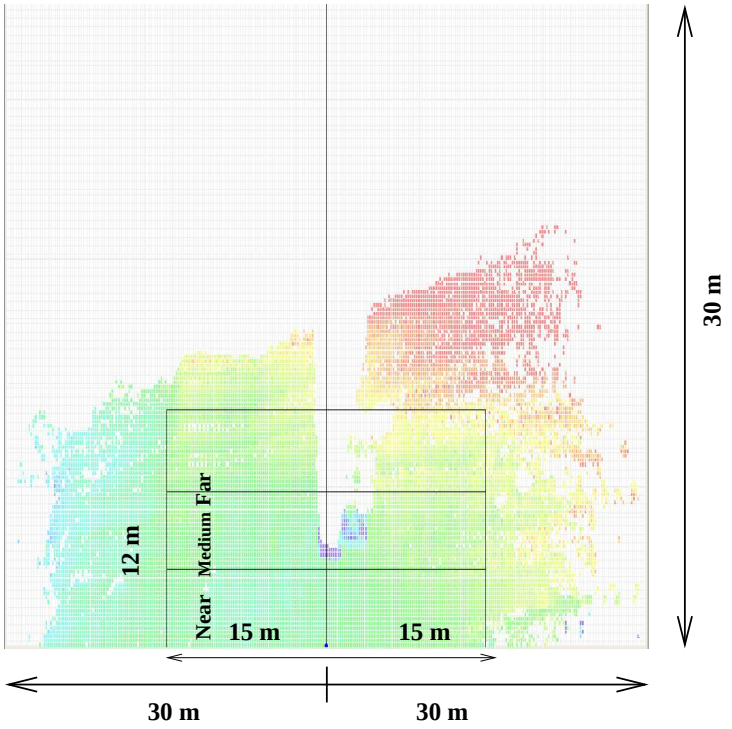

Figure 9: *Typical Ego-Centric Terrain Map*

culated for each map zone. The zone's average density is defined as the fraction of grid elements known:

$$\rho_{zone} = \frac{\sum_{i=1}^{N} grid\_defined_i}{N} \tag{6}$$

where N is the number of grid elements for the zone. This density is calculated for the entire map life, from the experiment's start to its completion. Life cycle statistics are used since they provide a better overall representation of the map's expected performance than could be achieved using a simple snapshot. A simple map snapshot is not reliable as it could yield unrealistically flattering or poor results.

The variance associated with an (x, y, z) point is proportional to its range [5]. Additionally, the variance for a grid element that contains only a single data point can not be calculated. Thus, for a single data point, which could be located anywhere within the grid element, its variance is specified as the size of the grid. The average zone variance is given by:

$$\sigma_{zone} = \frac{\sum_{i=1}^{N} \sigma_{grid_i}}{N} \tag{7}$$

where N is the number of grid elements for the zone. From the average variance the

average standard deviation may be calculated as: $\sqrt{\sigma_{zone}}$. This standard deviation is a statistical measure of the terrain map's overall quality because each individual grid element's standard deviation measures the goodness of the data, where a lower value indicates a higher confidence level and a higher standard deviation corresponds to less confidence in the data.

3.3 Initial Experiments

Previous investigations [14] using the Raptor UGV revealed poor terrain map performance, characterized by phantom obstacles produced by the traversibility analysis, for map sizes greater than approximately 15 m. Researchers hypothesized this poor performance resulted from the sparse sampling yielded by constant angular rate profile for nod angles less than $-10°$, but this hypothesis was untested. The experiments detailed in these sections investigate the terrain map performance issues and quantify the map's performance for a look-ahead distance of 12 m and corresponding laser angles of less or equal to $-10°$.

3.3.1 Map Performance, Single Fixed Laser

The first experiment used a single laser, which was set at four different fixed angles. Obviously, with the laser at a fixed angle vehicle motion is required to fully populate a terrain map. Figure 10 illustrates the egocentric terrain map obtainable from a stationary vehicle with a fixed laser angle. As can be seen in this figure the terrain map data is only available for the grid elements that were touched by the laser's scan. This figure also highlights this experiment's configuration, where the laser's look-ahead distance corresponds to the end of the far zone.

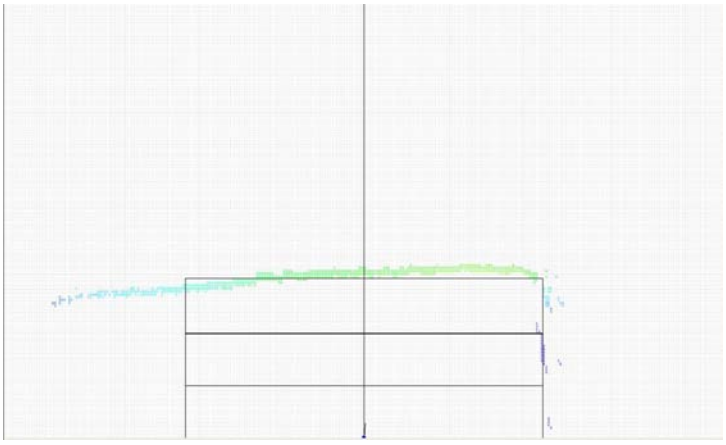

Figure 10: *Ego-Centric Terrain Map, Stationary Vehicle, Laser at* $-10°$

Figure 11 shows the egocentric map (left side), at the completion of the forward traverse, with the laser set at a fixed $-10°$ angle. As can be seen in this figure an obstacle is clearly visible. The figure's right portion shows egocentric map once the Raptor has returned to its starting position and the large blind zone is obvious.

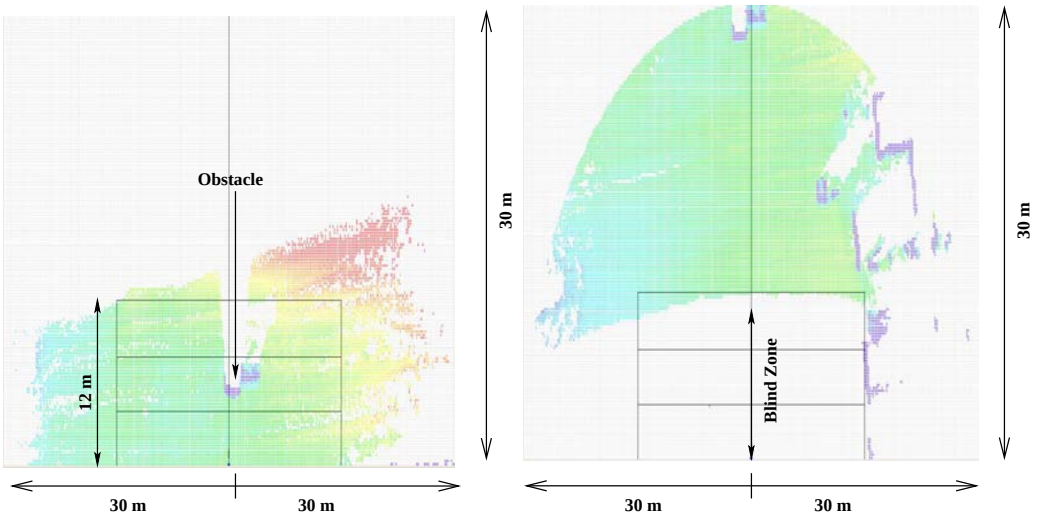

Figure 11: *Ego-Centric Terrain Map, Mid Traverse and Return to Start, Laser at* $-10°$

With the laser orientated at a $-20°$ angle the resulting egocentric map is more myopic, meaning it only represents terrain that is nearer to the vehicle. The egocentric map, resulting from the forward traverse, is shown on the left side in Figure 12.

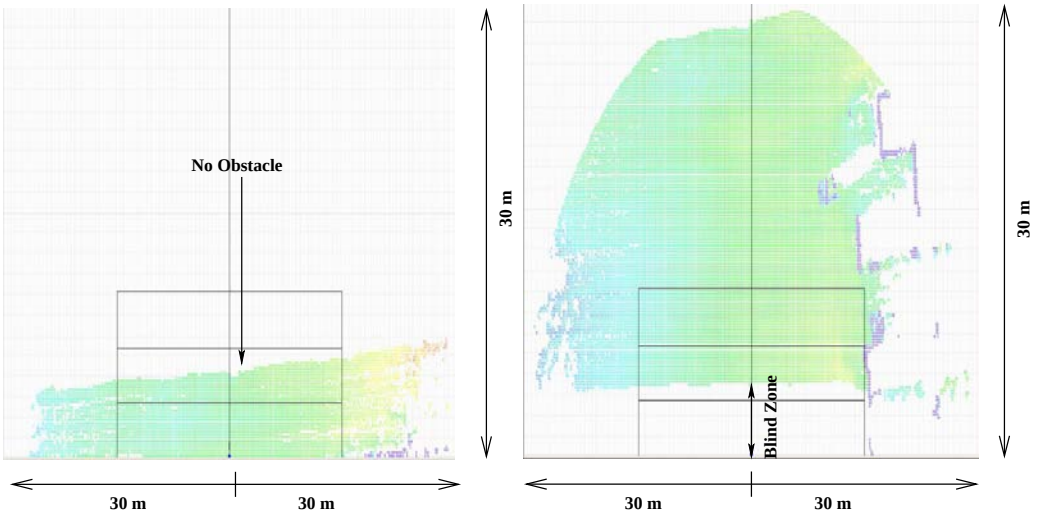

Figure 12: *Ego-Centric Terrain Map, Mid Traverse and Return to Start, Laser at* $-20°$

Whereas the laser mounted at the $-10°$ angle revealed an obstacle, as shown in Figure 11, this laser mount angle results in a short sighted map that is obstacle free. Although this egocentric map is myopic, the blind spot in front of the vehicle has been reduced, as shown by the map on the figure's right side.

Figure 13, left side, shows the egocentric map that results from the laser having an angle

of $-30°$ below the horizon. As can be seen in this figure, the corresponding egocentric map is extremely myopic as its look-ahead distance is only 4 m. Although this configuration results in a myopic egocentric map, the blind spot in front of the vehicle is significantly reduced, as can be seen in the map on the figure's right side.

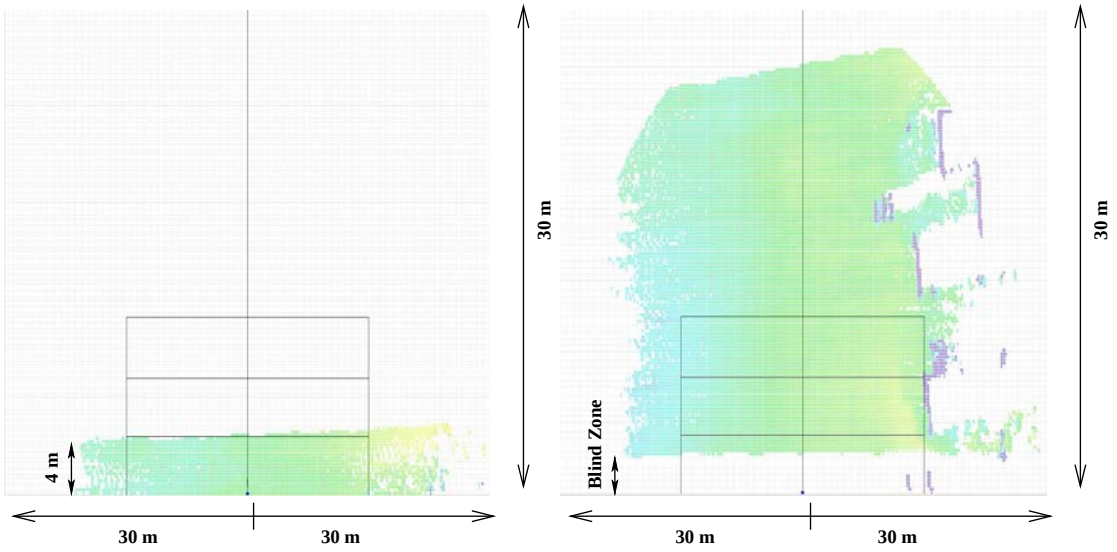

Figure 13: *Ego-Centric Terrain Map, Mid Traverse and Return to Start, Laser at $-30°$*

Although Figures 11 through 13 provide a useful visual representation, further analysis can provide other insights into how the laser mount angle influences the world representation. Table 2 shows the average known grid element density for the zones identified in Figure 9. Also included in Table 2 is the mean standard deviation of all valid grid elements, which is an indication of the map's overall *goodness*.

Config	**Angle**	**Rate**	**Near**		**Medium**		**Far**	
	Deg.	Deg/sec	Density	Std	Density	Std	Density	Std
Single	-10	0	57%	71	69%	71	68%	77
Single	-20	0	79%	56	32%	59	N/A	N/A
Single	-30	0	66%	58	N/A	N/A	N/A	N/A
Single	-40	0	42%	58	N/A	N/A	N/A	N/A

Table 2: *Single Laser, Forward Motion only*

Table 2 illustrates some obvious and some not so obvious terrain map traits:

- The map's far zone density is highly dependent upon the laser mount angle. With the laser set at $-10°$ the far zone's density is good, but other mounting angles result in a myopic map.
- When the laser is configured with a relatively short look-ahead distance, such as $-20°$

or -30° below the horizon, the map's density in the near zone improves while the next zone's density degrade[8].

- For a very short look-ahead distance of 2.5 m, which corresponds to -40°, the resulting terrain map is extremely myopic.

3.3.2 Map Performance, Dual Fixed Lasers

This experiment investigates the terrain map's performance when dual, fixed lasers acquire range data. The data set for this analysis is identical to the single, fixed laser experiment, but in this case both laser sources are used. Figure 14 shows a typical egocentric map that results from two fixed laser rangefinders. In this figure the angle between the laser angles is clearly shown.

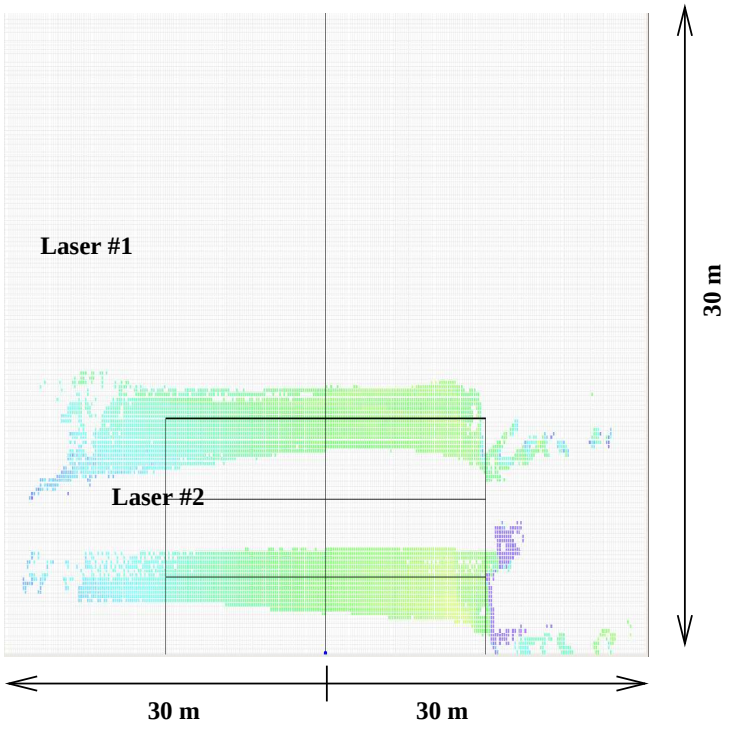

Figure 14: *Egocentric Map for Dual Lasers at -10° and -20°*

Table 3 reveals that the dual laser configuration results in a significant performance improvement. With a single laser, and only forward motion, certain zones were without any map information, as can be seen in Table 2. The addition of a second laser partially alleviates this problem. The two laser configuration also yielded overall higher data densities in all three map zones.

[8] Or no terrain map information is present.

Config	Angle #1	Angle #2	Rate	Near		Medium		Far	
	Deg.	Deg/sec	Deg.	Density	Std	Density	Std	Density	Std
Dual	-10	-10	0	59%	65	70%	64	81%	58
Dual	-10	-20	0	80%	56	75%	69	73%	69
Dual	-10	-30	0	79%	56	60%	73	70%	67
Dual	-10	-40	0	71%	63	62%	78	71%	61

Table 3: *Dual Lasers, Forward Motion only, Look-ahead distance 12 m*

3.3.3 Map Performance, Single Fixed Laser and a Nodding Laser

In Sections 3.3.1 and 3.3.2 the lasers were mounted at fixed angles and this setup requires vehicle motion in order to construct a populated terrain map. This configuration leads to a "chicken and egg" situation where the vehicle must move to create a terrain map, but it needs a populated terrain map *before* it moves so it can identify and avoid potential obstacles. The paradox has three common solutions:

- Use human input to ensure initial terrain in front of the vehicle is safe,
- Mount numerous lasers at fixed angles [3], and
- Scan the terrain in front of the vehicle by nodding a laser [4, 5].

Figure 15 shows a terrain map created by a nodding laser. This figure illustrates the nodding laser's ability to scan a region in front of a stationary vehicle.

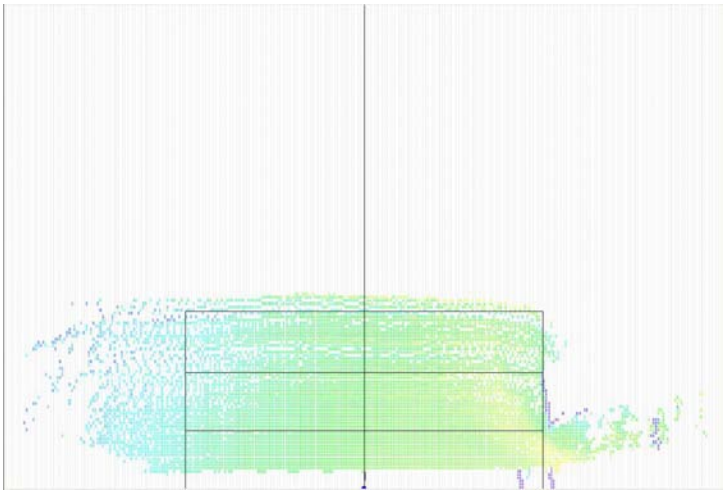

Figure 15: *Egocentric Map for a Nodding Laser, Stationary Vehicle*

Experiments were performed with one laser mounted at a fixed angle of $-10°$, while the second laser was nodded through various angles, at differing rotational rates. Table 4 lists the angles used for this experiment, and Table 5 provides the constant angular rates of rotational used in these experiments.

Experiment	**Low Angle**, Deg.	**High Angle**, Deg.
1	-40	-20
2	-40	-10
3	-40	-0

Table 4: *Nodding Angles for Experiments with a Fixed Laser Look-ahead distance of 12 m*

Trial	**Nod Rate**, Deg./s
1	5
2	10
3	15
4	15
5	25
6	30

Table 5: *Constant Angular Nodding Rates for the Experiments*

Table 6 shows the results when the nodding laser was configured to sweep the angle between $-40°$ and $-20°$. Given that the maximum nod angle is $-20°$, the nodding laser has a look-ahead distance of $\simeq 7$ m and never provides data for the far zone. This table reflects this configuration as it shows high data densities for the near zone, while the medium and far zones have lower data densities.

Config	**Angle**	**Rate**	**Near**		**Medium**		**Far**	
	Deg.	Deg/sec	Density	Std	Density	Std	Density	Std
Dual	-40 to -20	5	92%	64	91%	82	83%	83
Dual	-40 to -20	10	85%	59	68%	68	71%	66
Dual	-40 to -20	15	89%	62	66%	73	72%	67
Dual	-40 to -20	20	89%	59	68%	73	69%	69
Dual	-40 to -20	25	89%	61	71%	77	73%	73
Dual	-40 to -20	30	91%	63	72%	76	71%	73

Table 6: *Nod Angle $-20°$ to $-40°$, Fixed Laser Look-ahead distance 12 m*

The next experiment used a nodding angle between $-10°$ and $-40°$. This configuration allows the nodding laser to scan more distant terrain, thus it should improve the map's quality in the far zone. The experiment's results are shown in Table 7 and as was expected, allowing the laser to scan up to $-10°$ resulted in higher data densities for the medium and far zones.

For the final experiment the laser was nodded from the horizon down to $-40°$. The results of this experiment are given in Table 8. This configuration did not significantly affect the overall grid element densities, but did have a noticeable impact on the standard deviation associated with each grid element. The standard deviations of the medium zone often exceeded 80 mm and such a large value was rarely recorded in the previous experiments.

Config	Angle	Rate	Near		Medium		Far	
	Deg.	Deg/sec	Density	Std	Density	Std	Density	Std
Dual	-40 to -10	5	88%	58	79%	65	73%	61
Dual	-40 to -10	10	91%	61	82%	69	76%	68
Dual	-40 to -10	15	92%	57	87%	68	79%	64
Dual	-40 to -10	20	93%	56	90%	70	84%	74
Dual	-40 to -10	25	93%	57	90%	73	84%	77
Dual	-40 to -10	30	92%	59	95%	75	89%	80

Table 7: *Nod Angle -10° to -40°, Fixed Laser Look-ahead distance 12 m*

For the far zone the standard deviation reach values in excess of 90 mm. These high values are a result of nodding near the horizon, as the variance is directly proportional to the measured range and scanning this region yields longer range measurements.

Config	Angle	Rate	Near		Medium		Far	
	Deg.	Deg/sec	Density	Std	Density	Std	Density	Std
Dual	-40 to 0	5	88%	60	74%	68	73%	63
Dual	-40 to 0	10	90%	61	83%	75	76%	77
Dual	-40 to 0	15	84%	62	87%	83	83%	94
Dual	-40 to 0	20	90%	63	92%	85	86%	96
Dual	-40 to 0	25	88%	63	94%	83	87%	91
Dual	-40 to 0	30	89%	60	92%	82	86%	95

Table 8: *Nod Angle 0 to -40 Degrees, Fixed Laser Look-ahead distance 12 m*

3.3.4 Discussion

These initial experiments investigated the terrain map's performance for a relatively short look-ahead distance of approximately 12 m. From these investigations the following conclusions can be drawn:

- The single fixed angle laser configuration yielded the poorest map performance in terms of data densities. Additionally, this configuration was either myopic or suffered from a large blind zone.
- Dual fixed lasers performed better than the single laser configuration. The dual laser approach provided higher data densities, helped alleviate myopia and the blind zone problems associated with a single fixed laser, but still required vehicle motion to populate the terrain map.
- The single fixed laser and a single nodding laser configuration yielded the overall best results. This configuration was not myopic, didn't have a significant blind zone, nor did it require vehicular motion in order to build a map. For this configuration the

map's performance was largely independent of the nodding angles and the nodding rates.

3.4 Terrain Map Performance for a 24 m Look-ahead Distance

The initial experiments, detailed in Section 3.3, investigated the terrain map's performance for a conservative look-ahead distance of approximately 12 m. The experiments in this section investigate the terrain map's performance when the look-ahead distance is doubled to 24 m. Figure 16 shows the terrain map's configuration for this experiment. As in the previous experiments, the map is divided into three zones (near, medium and far), but for this set of experiments each zone is 8x30 m in size.

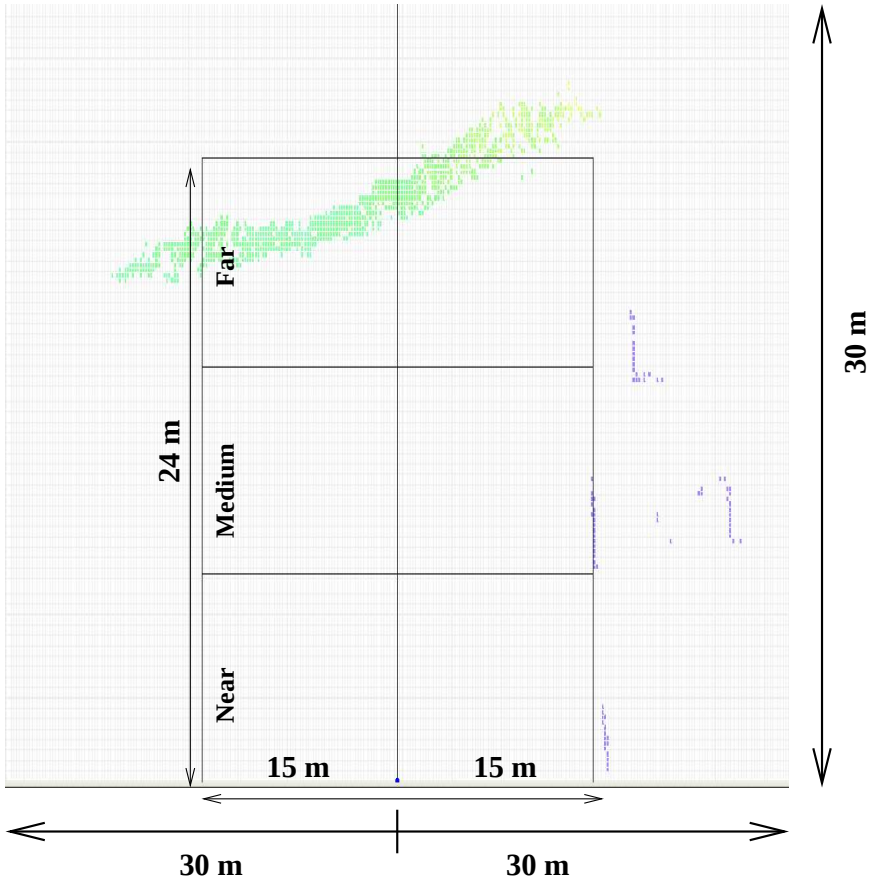

Figure 16: *Typical Ego-Centric Terrain Map with a 24 m Look-ahead distance*

In a manner similar to the previous experiments, the terrain map's performance was investigated for a single fixed laser, dual fixed lasers, and a fixed laser with a nodding laser under the CAR profile. These experiments also included a new mode of operation, the adaptive nodding mode, where the laser attempts to scan the terrain using the USD profile. The results of these experiments are presented in the following sections.

3.4.1 Map Performance, Single Fixed Laser

This experiment investigates a single laser's performance with a 24 m look-ahead distance and Table 9 shows results.

Config	Angle	Rate	Near		Medium		Far	
	Deg.	Deg/sec	Density	Std	Density	Std	Density	Std
Single	-5	0	18%	87	38%	95	54%	92
Single	-10	0	51%	59	70%	95	N/A	N/A
Single	-15	0	62%	59	5%	78	N/A	N/A
Single	-20	0	54%	56	N/A	N/A	N/A	N/A
Single	-25	0	42%	57	N/A	N/A	N/A	N/A
Single	-30	0	35%	58	N/A	N/A	N/A	N/A

Table 9: *Single Laser, Forward Motion only*

When compared to the single laser results presented in Table 2, this configuration performed poorly as the data densities were low and the data confidence was also low due to the higher standard deviations. These results are not surprising as each individual zone, at 8x30 m, is significantly larger than the 4.0x30 m zones used by the first set of experiments. Figure 17 illustrated this issue, where the left map has a 24 m look-ahead distance and the right map's look-ahead distance is 12 m.

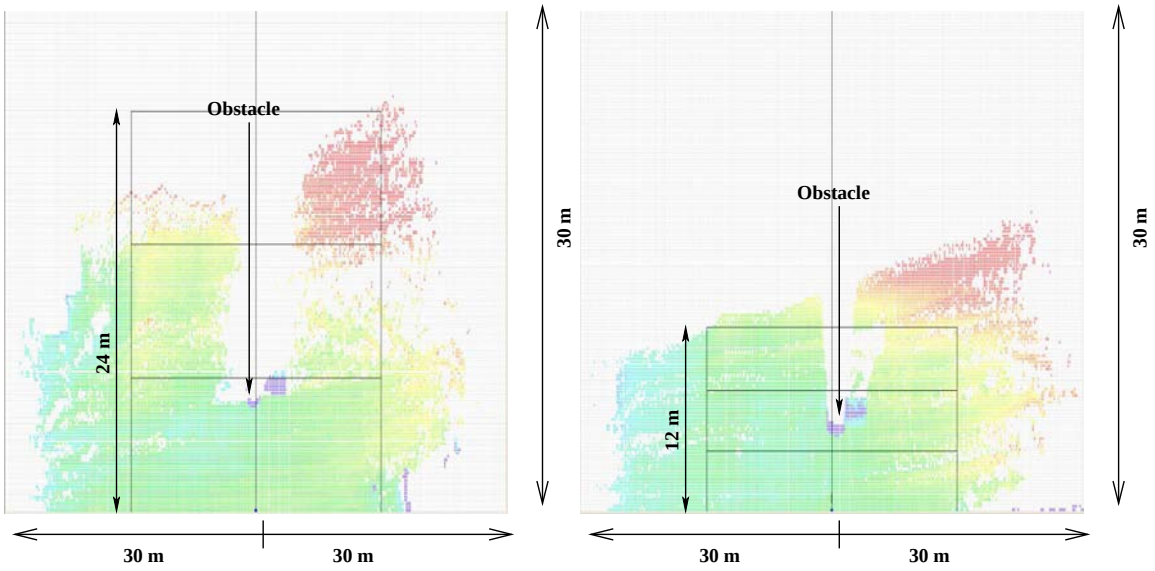

Figure 17: *Terrain Map with Zones, 24 M Look-ahead Distance (left) and 12 m Look-ahead Distance (right)*

3.4.2 Map Performance, Dual Fixed Lasers

This experiment investigates the terrain map's performance when dual, fixed lasers acquired range data. For these experiments one laser was fixed at -5° below the horizon, while the angle of the second laser was varied.

Config	**Angle**	**Rate**	**Near**		**Medium**		**Far**	
	Deg.	Deg/sec	Density	Std	Density	Std	Density	Std
Dual	5/5	0	25%	75	46%	83	63%	85
Dual	5/10	0	52%	57	60%	73	39%	108
Dual	5/15	0	64%	57	37%	96	37%	109
Dual	5/20	0	62%	59	36%	91	40%	105
Dual	5/25	0	56%	60	38%	90	40%	104
Dual	5/30	0	52%	69	40%	105	41%	115

Table 10: *Dual Lasers, Forward Motion only, Look-ahead distance 24 m*

Table 10 reveals that the dual laser configuration yields a significant performance improvement over the single laser performance given in Table 9. With the 24 m look-ahead distance the single laser configuration produced un-represented zones, while the dual laser setup provides for data in all zones. As expected, the data densities with the 24 m look-ahead distance are significantly lower than the data densities yielded by the 12 m look-ahead distance. Additionally, the data's standard deviations were significantly larger for this experiment and this effect is a direct result of the longer ranges.

3.4.3 Map Performance, Single Fixed Laser and a Nodding Laser

For these experiments one laser was configured at -5°, while the second laser was nodded through a specified sweep, at various constant rotational rates. Table 11 lists the angles used for this experiment, while the nodding rates were the same as those used for the 12 m look-ahead distance experiments and are listed in Table 5.

Experiment	**High Angle**, Deg.	**Low Angle**, Deg.
1	-30	-5
2	-25	-5
3	-20	-5
4	-15	-5

Table 11: *Nodding Angles for Experiments with a Fixed Laser Look-ahead distance of 24m*

Table 12 shows the results with the nodding laser configured to sweep the angle between -30° to -5° below the horizon. In this table the near zone has relatively high data densities with low standard deviations; the medium zone has moderate data densities and higher standard deviations; while the far zone has the lowest data densities and the highest standard deviations. This experiment also revealed the zone's data density and standard

deviation did not vary with the rotational rate. The exception to this trend is the 5°/s rate which exhibits unusually low grid element densities along with unusually small standard deviations.

Config	Angle	Rate	Near		Medium		Far	
	Deg.	Deg/sec	Density	Std	Density	Std	Density	Std
Dual	-30 to -5	5	78%	77	51%	103	44%	114
Dual	-30 to -5	10	85%	69	79%	118	54%	128
Dual	-30 to -5	15	85%	70	79%	118	57%	128
Dual	-30 to -5	20	87%	83	74%	128	57%	135
Dual	-30 to -5	25	87%	82	77%	127	56%	132
Dual	-30 to -5	30	89%	76	76%	122	56%	126

Table 12: *Nod Angle $-5°$ to $-30°$, Fixed Laser Look-ahead distance 24 m*

The next experiment used a nodding angle between $-25°$ and $-5°$ and the results are shown in Table 13. This experiment's results are very similar to the previous experiment reported in Table 12.

Config	Angle	Rate	Near		Medium		Far	
	Deg.	Deg/sec	Density	Std	Density	Std	Density	Std
Dual	-25 to -5	5	80%	71	63%	96	49%	112
Dual	-25 to -5	10	86%	70	76%	114	54%	124
Dual	-25 to -5	15	85%	73	82%	121	56%	130
Dual	-25 to -5	20	85%	68	81%	118	62%	131
Dual	-25 to -5	25	87%	72	80%	118	56%	128
Dual	-25 to -5	30	85%	70	81%	120	59%	132

Table 13: *Nod Angle $-5°$ to $-25°$, Fixed Laser Look-ahead distance 24 m*

Table 14 shows the results for the experiment that used a $-20°$ to $-5°$ nod angle. Given that the laser nods closer to the horizon, this experiment should show lower data densities in the near zone and higher data densities in the far zone, and the table shows this effect.

Config	Angle	Rate	Near		Medium		Far	
	Deg.	Deg/sec	Density	Std	Density	Std	Density	Std
Dual	-20 to -5	5	71%	61	86%	94	60%	122
Dual	-20 to -5	10	82%	67	84%	111	61%	133
Dual	-20 to -5	15	80%	59	85%	102	64%	119
Dual	-20 to -5	20	81%	68	82%	110	62%	124
Dual	-20 to -5	25	84%	74	82%	116	61%	130
Dual	-20 to -5	30	82%	76	82%	120	61%	131

Table 14: *Nod Angle $-5°$ to $-20°$, Fixed Laser Look-ahead distance 24 m*

The final experiment under this configuration nodded the laser between the angles of $-15°$ and $-5°$. Given that this configuration focuses on terrain that is far from the Raptor UGV, the terrain in this region should be better represented. Table 15 verifies these expectations as the far and medium zone's data densities are higher than found under the previous experiments.

Config	**Angle**	**Rate**	**Near**		**Medium**		**Far**	
	Deg.	Deg/sec	Density	Std	Density	Std	Density	Std
Dual	-15 to -5	5	61%	36	91%	70	67%	122
Dual	-15 to -5	10	70%	52	88%	89	69%	124
Dual	-15 to -5	15	69%	63	89%	96	63%	125
Dual	-15 to -5	20	71%	62	90%	95	66%	125
Dual	-15 to -5	25	72%	58	90%	95	67%	121
Dual	-15 to -5	30	72%	64	86%	101	65%	121

Table 15: *Nod Angle $-5°$ to $-15°$, Fixed Laser Look-ahead distance 24 m*

Although this configuration better represents the medium and far regions, the near region is not as well represented and the vehicle's blind spot is significant. Calculations show the this configuration should have a blind spot of 7.8 m as can be seen in Figure 18.

3.4.4 Map Performance, Adaptive Nodding

The final set of experiments exercised an adaptive nodding mode where the laser dynamically changes its nodding rate in order to maintain a uniform sample distance. For these experiments the uniform sample distance was set at 0.2 m, a value that matches the terrain map's grid size. The results of this experiment are given in Table 16. This table reveals some very interesting results when compared to the previous experiments with the same sweep angles. When compared with the CAR profile the USD profile features marginally lower data densities, along with lower standard deviations. The lower data densities are counterintuitive, however, the lower standard deviations are the more important fact as it is a measure of the data's quality and indicates that the map's quality has improved.

Config	**Low Angle**	**High Angle**	**Near**		**Medium**		**Far**	
	Deg.	Deg.	Density	Std	Density	Std	Density	Std
Adaptive	-5	-10	57%	74	80%	85	69%	113
Adaptive	-5	-15	59%	47	76%	73	67%	103
Adaptive	-5	-20	81%	59	79%	81	51%	101
Adaptive	-5	-25	79%	64	72%	79	51%	106
Adaptive	-5	-30	86%	62	69%	85	49%	103

Table 16: *Dual Lasers, Adaptive Nodding, Look-ahead distance 24 m*

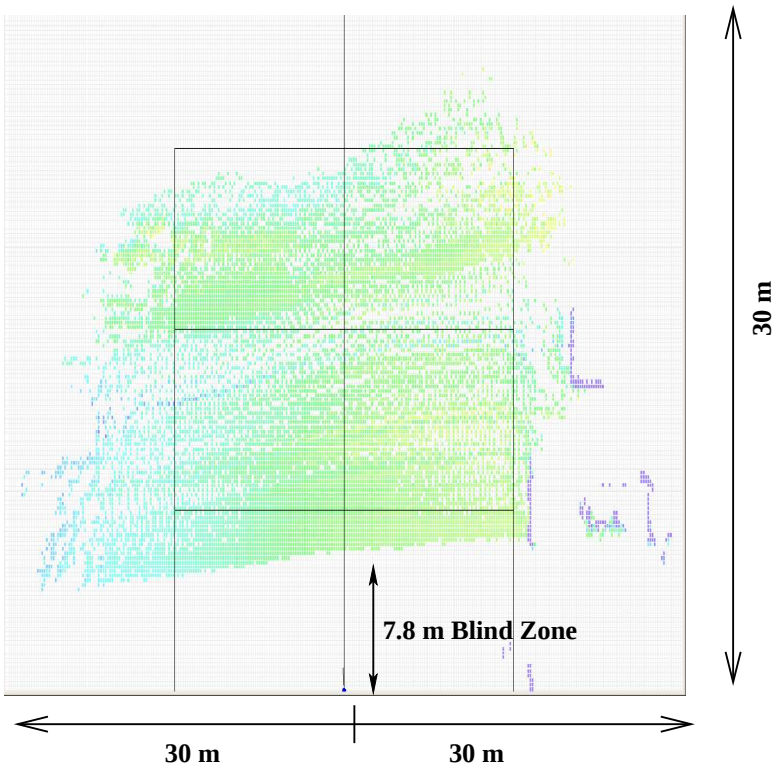

Figure 18: *Terrain Map with Zones, Nod Angle* $-5° \rightarrow -30°$

3.4.5 Discussion

The conclusions drawn from these experiments are similar to those drawn from the 12 m look-ahead distance experiments presented in Section 3.3. Namely, dual lasers perform better than a single laser and a nodding laser has the additional benefit of producing a populated terrain map without the need for vehicular motion.

These experiments also compared the CAR profile with the USD profile. The experiments revealed that the adaptive nodding, under the USD profile, slightly reduced both the grid element data densities and their associated standard deviations. This effect was observed for all map zones and across nodding angles with the most notable effect on the far zone, while the near zone showed the least effect. The reduced standard deviation can be attributed to the scanning process, where a grid element that contains only a single data point is given a relatively high standard deviation of 200 mm. The adaptive nodding configuration spends more time nodding near the horizon and, thus, helps ensure that more grid elements have multiple data points. This in turn reduces the overall standard deviation, which results in an better map from a statistical perspective. Given that all map zones show a decreased data density the underlying cause must be systematic in nature. The vehicle's forward velocity, in conjunction with the slow rotation rates of the the USD profile may be mechanism that causes the lower data densities. With one laser fixed and the second laser nodding slowly

the forward movement could result in terrain patches that are not sampled. The CAR profile experiments, shown in Tables 12 to 18 bolster this hypothesis as they all show that lower data densities are correlated with slower rotational rates.

4 Conclusions

A number of experiments have been conducted examining the performance of a single laser configuration, the dual laser configuration, the CAR profile and the USD profile. Based upon previous experience and theoretical investigations, Defence R&D Canada researchers' had concluded that data densities are a key factor in producing statistically sound terrain maps. These experiments verified this *a priori* assumption and contributed a number of new insights into terrain sampling approaches.

First, more lasers result in higher sampling densities, which in turn yield better quality terrain maps. The map quality is quantitatively better in terms of the known to unknown grid element ratio and with respect to the data confidence as given by the grid element's standard deviation.

Secondly, all fixed laser configurations resulted in either a myopic map or a map that suffered from a blind zone where no map data was present. Additionally, the fixed laser configuration required vehicular motion in order to adequately populate the terrain map with data.

Thirdly, the single fixed laser with a single nodding laser configuration proved to be superior to any fixed laser configuration as it can populate the map while the vehicle is stationary. Additionally, this configuration provided better quality terrain maps through higher data densities and greater confidence in the map data. These investigations also revealed that the map quality was not overly dependent on the nodding angles and the nodding rates, thus the researcher is free to use a configuration that minimizes the blind zone, while maximizing the look-ahead distance.

Finally, a comparison was made between a laser nodding under the CAR profile and a laser using the adaptive USD profile. This comparison revealed that the adaptive nodding configuration yielded a better quality map, from statistical perspective as the zone standard deviations were lower than was produced by nodding at a constant angular rate. It was also noted that the current USD profile exhibited lower data densities and it was hypothesized that this counterintuitive result stemmed from an interaction between the vehicle's velocity and the slow nodding rate of the USD profile. Future research could investigate dynamically adjusting the USD profile so that the algorithm compensates for the vehicle's velocity.

Additonally, these experiments addressed the issue of the maximum usable look-ahead distance. During DRDC's fall 2005 Raptor demonstration researchers experienced difficulties with look-ahead distances of greater than 15 m, where the traversibility analysis produced phantom obstacles. These experiments revealed no statistical basis for a poorer terrain map performance with a 24 m look-ahead distance. The longer look-ahead distance resulted in

lower map zone densities and larger grid element standard deviations, but these differences are a result of the system's geometry and were predicted by theory. With the appropriate traversibility analysis, the Raptor UGV should operate near the maximum SICK laser range of 30 m and, thus, allow the Raptor to aim high in steering. This in turn would improve obstacle avoidance manoeuvres by allowing the Raptor to make longer range decisions.

This report has shown that the laser configuration has a significant impact on terrain map construction. Although the configuration had a large impact, the most significant factor is the range data densities that are available. More range data yields a terrain map that has improved statistical properties. Future research avenues include acquiring laser rangefinders with higher data densities and then comparing the resulting terrain map performance with DRDC's current configuration.

References

[1] Collier, J, Broten, G., and Giesbrecht, J. (2006), Traversibility Analysis for Unmanned Ground Vehicles, (DRDC Suffield TM 2006-175) Defence R&D Canada – Suffield, P.O. Box 4000, Station Main, Medicine Hat, Albe.

[2] Broten, G., Giesbrecht, J., and Monckton, S. (2005), World Representation Using Terrain Maps, (DRDC Suffield TR 2005-248) Defence R&D Canada – Suffield, Medicine Hat, Alberta.

[3] Thrun, S., Montemerlo, M., Dahlkamp, H., Stavens, D., Aron, A., Diebel, J., Fong, P., Gale, J., Halpenny, M., Hoffmann, G., Lau, K., Oakley, C., Palatucci, M., Pratt, V., Stang, P., Strohband, S., Dupont, C., Jendrossek, L.-E., Koelen, C., Markey, C., Rummel, C., van Niekerk, J., Jensen, E., Alessandrini, P., Bradski, G., Davies, B., Ettinger, S., Kaehler, A., Nefian, A., and Mahoney, P. (2006), Stanley: The Robot That Won the DARPA Grand Challenge, *Journal of Field Robotics*, 23(9), 661–692.

[4] Broten, G. and Collier, J. (2006), Continuous Motion, Outdoor, 2 1/2D Grid Map Generation using an Inexpensive Nodding 2-D Laser Rangefinder, In *Proceedings of the 2006 IEEE International Conference on Robotics and Automation*, Number 2006-061, pp. 4240–4245, Orlando, Fl.

[5] Broten, G. and Collier, J. (2005), The Characterization of an Inexpensive Nodding Laser, (DRDC Suffield TR 2005-232) Defense R&D Canada – Suffield, Medicine Hat, Alberta.

[6] (2005), RTEMS Website. www.rtems.com/features.

[7] (2006), RTEMS Development Host Tools and RTEMS Source Code. http://www.rtems.com/down.html.

[8] Broten, Greg (2006), DRDC – Suffield AISS Wiki HOWTO for installing RTEMS for the M68360. http://mao/wiki/index.cgi?RTEMS_68360.

[9] Utz, H., Sablatnog, S., Enderle, S., and Kraetzschmar, G. (2002), Miro - MIddleware for Mobile Robot Applications, *IEEE Transactions on Robotics and Automation*.

[10] Enderle, S., Utz, H., Sablatnog, S., Simon, S., Kraetzschmar, G., and Palm, G. (2001), Miro - Middleware for Autonomous Mobile Robots, *International Federation of Automatic Control*.

[11] Broten, G., Collier, J., Giesbrect, J., Monckton, S., and Mackay, D. (2006), The Architecture for Autonomy, (DRDC Suffield TM 2006-188) Defence R&D Canada – Suffield, P.O. Box 4000, Station Main, Medicine Hat, Alberta.

[12] Broten, G., Monckton, S., Giesbrecht, J., and Collier, J. (2006), Software Sysetms for Robotics, An Applied Research Perspective, *International Journal of Advanced Robotic Systems*, Volume 3, 1(2005-204), 11–17.

[13] Broten, G. and Monckton, S. (2005), Frameworks and Middleware for Unmanned Ground Vehicles, In *Proceedings of the UGV Technology Conference at the 2005 SPIE Defense and Security Symposium*, Number 2005-058, pp. 655–664, Orlando, FL.

[14] Monckton, S., Collier, J., Giesbrecht, J., Broten, G., Mackay, D., Erickson, D., Verret, S., and Digney, B. (2006), The ALS Project: Lessons Learned, In Gerhart, G. R., ShoeMaker, C.M., and Gage, D.M., (Eds.), *SPIE Defense and Security Symposium Unmanned Systems Technology VIII*, Vol. 6230, p. 12.

Distribution list

DRDC Suffield TM 2007-295

Internal distribution

DRDC - Suffield

1 DG/DDG/Ch. Sci./SMO

1 H/AISS

2 Lead Author

2 Library - 1 hardcopy/1 softcopy

Other DRDC

1 DRDKIM - CD

Total internal copies: 7

Total copies: 7

This page intentionally left blank.

DOCUMENT CONTROL DATA

(Security classification of title, body of abstract and indexing annotation must be entered when document is classified)

1. ORIGINATOR (The name and address of the organization preparing the document. Organizations for whom the document was prepared, e.g. Centre sponsoring a contractor's report, or tasking agency, are entered in section 8.)

   Defence R&D Canada – Suffield
   PO Box 4000, Medicine Hat, AB, Canada T1A 8K6

2. SECURITY CLASSIFICATION (Overall security classification of the document including special warning terms if applicable.)

   UNCLASSIFIED

3. TITLE (The complete document title as indicated on the title page. Its classification should be indicated by the appropriate abbreviation (S, C or U) in parentheses after the title.)

   Profiles for Nodding Lasers- Implementations and Results

4. AUTHORS (Last name, followed by initials – ranks, titles, etc. not to be used.)

   G. Broten,

5. DATE OF PUBLICATION (Month and year of publication of document.)

   December 2007

6a. NO. OF PAGES (Total containing information. Include Annexes, Appendices, etc.)

   42

6b. NO. OF REFS (Total cited in document.)

   14

7. DESCRIPTIVE NOTES (The category of the document, e.g. technical report, technical note or memorandum. If appropriate, enter the type of report, e.g. interim, progress, summary, annual or final. Give the inclusive dates when a specific reporting period is covered.)

   Technical Memorandum

8. SPONSORING ACTIVITY (The name of the department project office or laboratory sponsoring the research and development – include address.)

   Defence R&D Canada – Suffield
   PO Box 4000, Medicine Hat, AB, Canada T1A 8K6

9a. PROJECT NO. (The applicable research and development project number under which the document was written. Please specify whether project or grant.)

9b. GRANT OR CONTRACT NO. (If appropriate, the applicable number under which the document was written.)

10a. ORIGINATOR'S DOCUMENT NUMBER (The official document number by which the document is identified by the originating activity. This number must be unique to this document.)

   DRDC Suffield TM 2007-295

10b. OTHER DOCUMENT NO(s). (Any other numbers which may be assigned this document either by the originator or by the sponsor.)

11. DOCUMENT AVAILABILITY (Any limitations on further dissemination of the document, other than those imposed by security classification.)

   (X) Unlimited distribution
   ( ) Defence departments and defence contractors; further distribution only as approved
   ( ) Defence departments and Canadian defence contractors; further distribution only as approved
   ( ) Government departments and agencies; further distribution only as approved
   ( ) Defence departments; further distribution only as approved
   ( ) Other (please specify):

12. DOCUMENT ANNOUNCEMENT (Any limitation to the bibliographic announcement of this document. This will normally correspond to the Document Availability (11). However, where further distribution (beyond the audience specified in (11)) is possible, a wider announcement audience may be selected.)

   Unlimited

13. ABSTRACT (A brief and factual summary of the document. It may also appear elsewhere in the body of the document itself. It is highly desirable that the abstract of classified documents be unclassified. Each paragraph of the abstract shall begin with an indication of the security classification of the information in the paragraph (unless the document itself is unclassified) represented as (S), (C), (R), or (U). It is not necessary to include here abstracts in both official languages unless the text is bilingual.)

Historically, Defence R&D Canada investigated tele-operated vehicles, but in 2002 its research focus moved to general autonomy for land, air, and sea craft. Autonomy demands that the unmanned vehicle sense and represent its world as a prerequisite to intelligent navigation. A key element of Defence R&D Canada – Suffield's sensing suite is the nodding laser rangfinder that DRDC developed in conjunction with Scientific Instrumentation Ltd. The laser range data, returned from the nodding SICK laser, is the primary data source for DRDC's $2\frac{1}{2}$ D grid-map-based world representation. In its original form, the SICK laser nodded at a constant angular rate nodding profile. This implementation proved adequate for the fall 2005 Autonomous Land Systems demonstration, but the original implementation was utilitarian in nature. Although the constant angular rate nodding profile has yielded admirable results, analysis has shown that an adaptive nodding rate should theoretically yield even better results. Researchers at DRDC modified the nodding device's software to support user-definable, adaptive nodding profiles. Field tests exercised the new embedded software and revealed that the adaptive nodding system performed correctly. Experiments were then conducted to compare the performance of the constant angular rate profile to the performance of the adaptive nodding profile. These experiments revealed the performance of the adaptive nodding profile to be superior to that of the constant angular rate profile and the results were consistent with those predicted by theory and simulation.

14. KEYWORDS, DESCRIPTORS or IDENTIFIERS (Technically meaningful terms or short phrases that characterize a document and could be helpful in cataloguing the document. They should be selected so that no security classification is required. Identifiers, such as equipment model designation, trade name, military project code name, geographic location may also be included. If possible keywords should be selected from a published thesaurus. e.g. Thesaurus of Engineering and Scientific Terms (TEST) and that thesaurus identified. If it is not possible to select indexing terms which are Unclassified, the classification of each should be indicated as with the title.)

laser rangefinder, unmanned ground vehicle, sensing, perception, terrain maps, adaptive nodding

Defence R&D Canada

Canada's Leader in Defence
and National Security
Science and Technology

R & D pour la défense Canada

Chef de file au Canada en matière
de science et de technologie pour
la défense et la sécurité nationale

www.drdc-rddc.gc.ca